EXPERIMENTAL EVALUATION ON A MACH-SCALED SNUF BLADE FOR ACTIVE VIBRATION CONTROL

ByeongUk Im, goody147@snu.ac.kr, Seoul National University (Korea, Republic of)

ChangBae Lee, lcb_109@snu.ac.kr, Seoul National University (Korea, Republic of)

SangJoon Shin, ssjoon@snu.ac.kr, Seoul National University (Korea, Republic of)

Abstract

Seoul National University Flap (SNUF) blade equipped with an active trailing-edge flap is fabricated and tested under static conditions. Bench tests on the flap mechanism reveal the control authority and endurance of the devised flap actuation mechanism while centrifugal load acts on the flap. Also, the frequency response of the flap mechanism is identified where the static load is imposed on the flap. Blade tensile tests are performed for each root and flap component separately. Each specimen shows greater than 40% of safety margin compared with the expected maximum centrifugal load from comprehensive rotor analysis. The axial stiffness estimated from the measured skin strain is in good agreement with the cross-sectional analysis. Basic properties tests on the fabricated blade are carried out. Both sectional strain measurements and the identified modal frequencies show similar discrepancies in the flapping and torsional directions, which are 4% and 20% differences with design analysis, respectively. Finally, estimated MAC values for the first three fundamental modes satisfy the rejection criteria of 0.9.

1. INTRODUCTION

Recent studies have demonstrated that individual blade control (IBC) using either the active twist rotor (ATR) or active trailing-edge flaps (ATEFs) are capable of reducing rotorcraft vibration [1-3]. With the technological advances in smart material actuator such as piezoelectric actuator, small- and full-scale blades with ATEFs have been designed and tested on whirl towers and in flight [4-9]. Such flapped blades require integrated blade design that takes into account elaborated dynamics of the blade and the flap components due to increased load by addition of the flap driving mechanism.

For the last few years, the Mach-scaled active flap blade named as SNUF blade was created through an optimized design framework including comprehensive rotor analysis, computational fluid dynamics analysis and detailed blade structural analysis [10-13]. The flap driving mechanism was fabricated and tested under expected static centrifugal load for more than two hours without piezoelectric actuator [11]. Further, characteristics of the linear-periodic flap rotor system were investigated [14].

Copyright Statement

The authors confirm that they, and/or their company or organization, hold *copyright on all of the original material included in this paper. The authors also confirm that they have obtained permission, from the copyright holder of any third party material included in this paper, to publish it as part of their paper. The authors confirm that they give permission, or have obtained permission from the copyright holder of this paper, for the publication and distribution of this paper as part of the ERF proceedings or as individual offprints from the proceedings and for inclusion in a freely accessible web-based repository*.

In this paper, experimental studies of SNUF blade are conducted. Test results are compared with those of the three-dimensional and the one-dimensional structural analysis to verify the design. Typical results include static and dynamic ones on the fabricated active blade and flap driving mechanism with piezoelectric actuator, and modal tests with analytical model validation.

2. EXPERIMENT AND ANALYSIS ON SNUF BLADE

2.1. SNUF blade specifications

SNUF blade has a NACA0015 airfoil cross-section with a rectangular planform. A 15%c trailing-edge flap is located from 65% to 85% span station. Tip Mach number is set to 0.6, and the radius is 1.5 m. Figure 1 shows the cross-sectional configuration, spanwise planform and photos of fabricated SNUF blade.

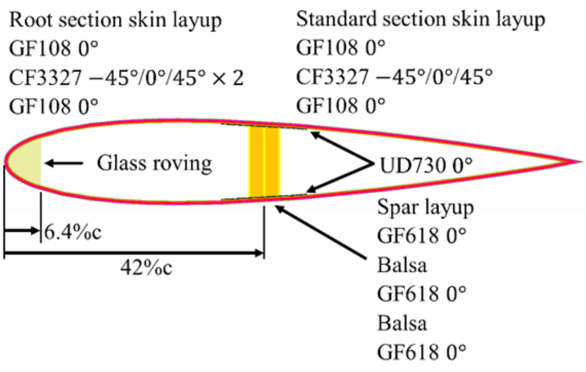

(a) Cross-section of SNUF blade

Presented at 45th European Rotorcraft Forum, Warsaw, Poland, 17-20 September, 2019

This work is licensed under the Creative Commons Attribution International License (CC BY). Copyright © 2019 by author(s).

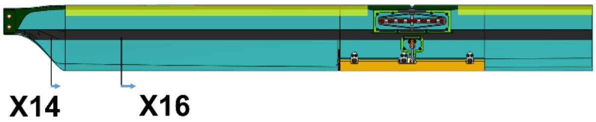

(b) Planform of SNUF blade

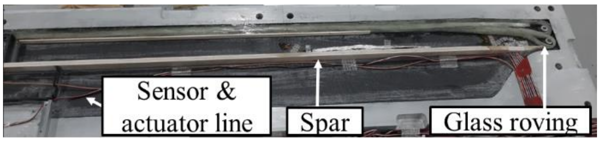

(c) Fabricated structures of blade on mould

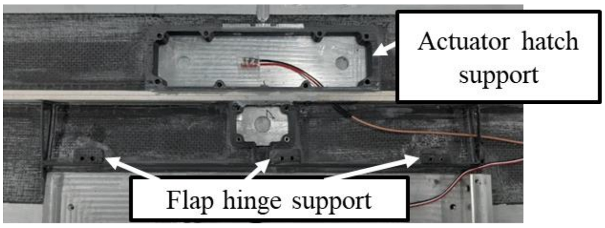

(d) Flap section view

(e) Fabricated blade

Figure 1. SNUF blade configuration.

2.2. Experimental methods and setup

At first, a frequency sweep actuating test of the active flap mechanism and an endurance test imposing 200N centrifugal load on the flap are conducted at the bench experiment. Figure 2 (a)–(c) show the bench experiment setup for the present flap driving system. In Fig. 2-(b), span-wise and chord-wise strains are measured at the flap carbon fabric, and span-wise strain of a shaft guide is monitored. Flap angle is measured by a potentiometer.

Structural integrity of the prototype blade is verified by tensile tests on an universal testing machine. The blade is stretched upto 25kN tensile load, for the maximum expected centrifugal load is 20kN at the blade root section.

Blade tensile specimen is divided into a root and a flapped component. Tensile load schedule is organized according to the University of Michigan blade tensile testing procedure [15]. A pretension of 50N is imposed to match the starting condition. Then, the crosshead of testing machine is moved with constant speed of 0.0254 mm/s, until the load becomes maximum 25kN. Specifically, the flap is driven with 5Hz sinusoidal signal during the test, and the flap deflection is measured with laser sensor to check whether any performance degradation of active flap happens.

Figure 3-(b) shows installed strain gauges on the blade skin. Two strain rosettes were attached on the 25% chord line, one at 25%R and the other at 38%R for the root part specimen. The strain rosette measures 0° and 90° direction strains. Each corresponds to X14 and X16 cross-sections in Fig. 1-(b). Also, in Fig. 3-(c), the flap component specimen has one 25% chord strain rosette, and the other rosette is installed near the flap cut-out section where stress concentration is expected. All the strain gauges are in quarter bridge configuration.

Finally, basic structural properties of the fabricated master blade is measured and compared with the analysis used for the blade design. Sectional bending and torsional stiffness are measured at a cantilevered experiment with tip load. Also, a modal test is conducted at free-free boundary condition where the blade is hanged with a nylon string.

Mode shape is identified from the frequency response function measured with an accelerometer by impact hammer roving test. The test only includes only perpendicular impacts on the blade surface to get flap bending and torsional modes. Figure 4 (a)–(d) shows each test setup.

The measurement equipment for bench and tensile test is configured using two synchronized NI-PCI 6281 DAQ board with a desktop (Intel i7, 4.2 GHz), NI SCXI-1000 chassis and SCXI-1314/1520 strain gauge bridge circuit boards. Data are acquired at 75/rev (1624.8 Hz) where the real time execution loop is constructed by Visual C++. In the modal test, NI-PXI 1042Q gets acclerometer and impact signals at 25kHz sampling frequency.

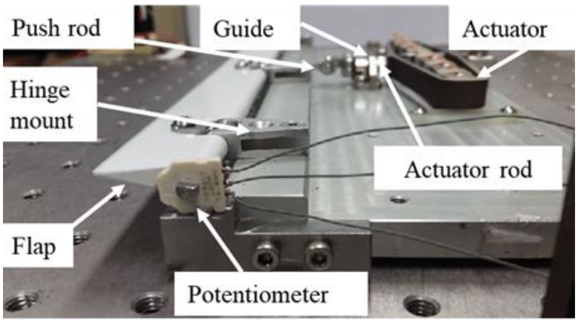

(a) Close view of the flap mechanism

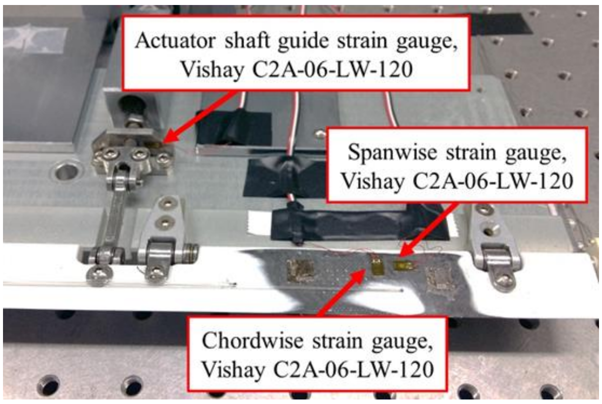

Presented at 45th European Rotorcraft Forum, Warsaw, Poland, 17-20 September, 2019
This work is licensed under the Creative Commons Attribution International License (CC BY). Copyright © 2019 by author(s).

(b) Installed strain gauges on the flap mechanism

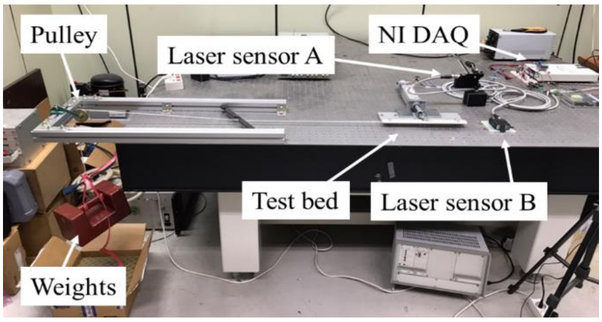

(c) Endurance test setup

Figure 2. Bench experiment setup

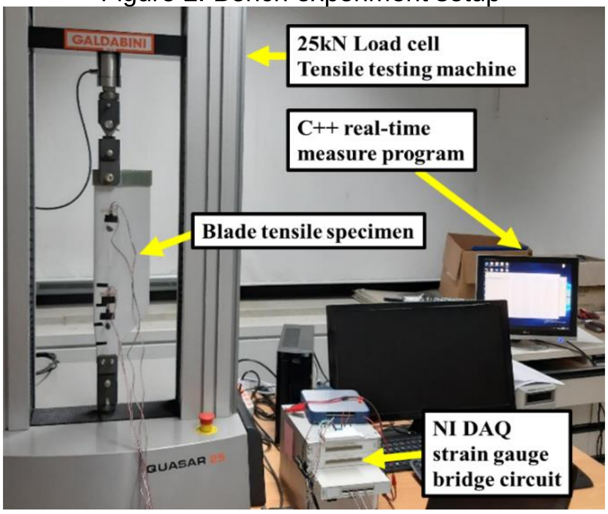

(a) Blade tensile load test equipments

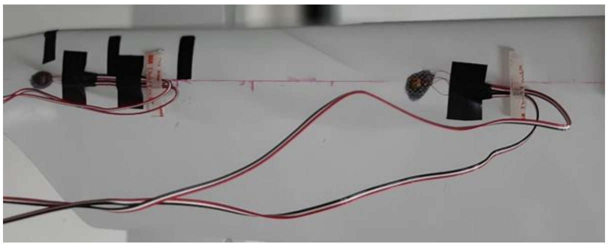

(b) Installed strain gauges on the root specimen

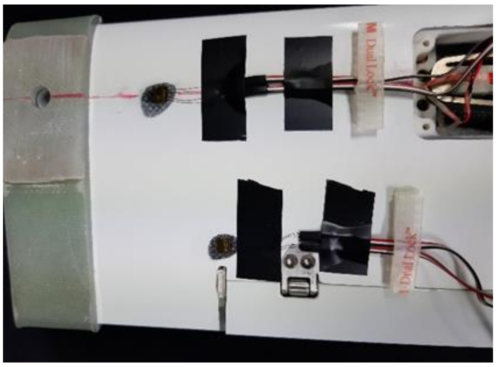

(c) Installed strain gauges on the flap specimen

Figure 3. Tensile load test setup

(a) Flap bending stiffness test

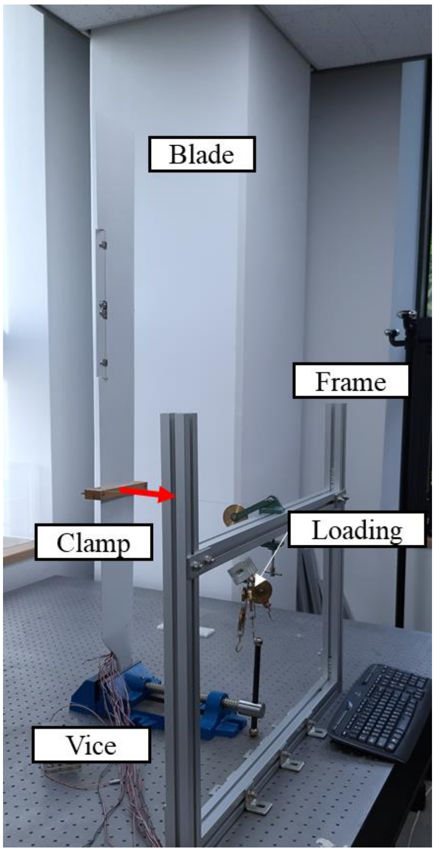

(b) Torsional stiffness test

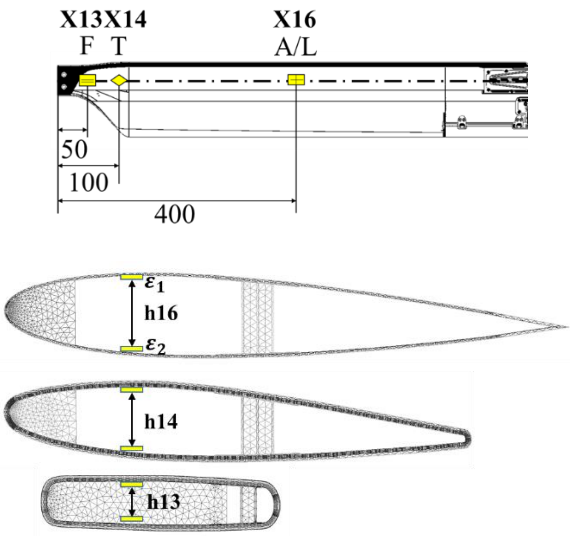

(c) Strain gauge installation locations

Presented at 45th European Rotorcraft Forum, Warsaw, Poland, 17-20 September, 2019

This work is licensed under the Creative Commons Attribution International License (CC BY). Copyright © 2019 by author(s).

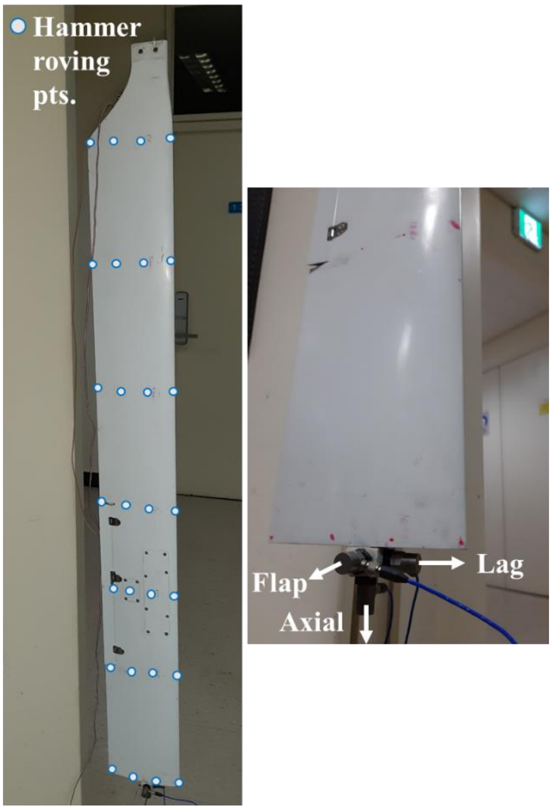

(d) Modal test setup

Figure 4. Blade structural properties test

2.3. Test results and evaluation

2.3.1. Basic blade properties test

As a preliminary test, blade mass and chord-wise center of gravity (CG) are measured to validate the inertial properties used for design with actual fabrication. Figure 5-(a) shows the measured blade mass of 1.13 kg, which has 3.5% difference with the designed mass estimated by VABS [18]. Thus, present analytical density properties predicted by the combination of fabric and epoxy resin are found to be accurate. The corresponding Lock number is approximately 4.8. Chord-wise CG is estimated by static balancing the blade on a slim support.

(a) Blade mass measurement

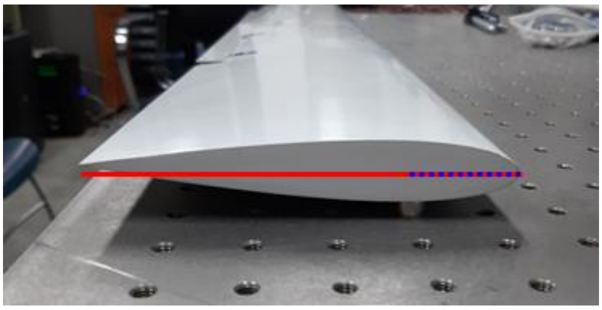

(b) Blade chord-wise center of gravity measurement

Figure 5. Basic properties test

In Fig. 5-(b), the red solid line indicates complete blade chord, and blue dashed line is depicted with exact 25%c. Then, it is concluded that the blade has its chord-wise CG near 25%c, which matches with design point.

2.3.2. Endurance test on flap mechanism

Endurance test on the flap mechanism was performed in the previous research, but it was without the strain measurements on the flap or any driving structures [11]. The purpose of this additional test is to assess the strains during 10 min of static equilibrium loading conditions using the piezoelectric actuator.

Figure 6 (a)–(c) depicts the resulting strains after 10 minutes. Static strains of carbon flap had increased in both directions, and the strain of steel shaft guide had also amplified. Measured strains are sufficiently small compared to the allowable strain limits.

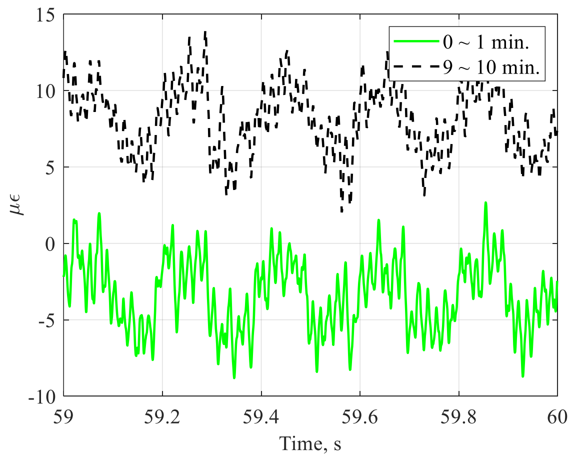

(a) Flap span-wise gauge

Presented at 45th European Rotorcraft Forum, Warsaw, Poland, 17-20 September, 2019

This work is licensed under the Creative Commons Attribution International License (CC BY). Copyright © 2019 by author(s).

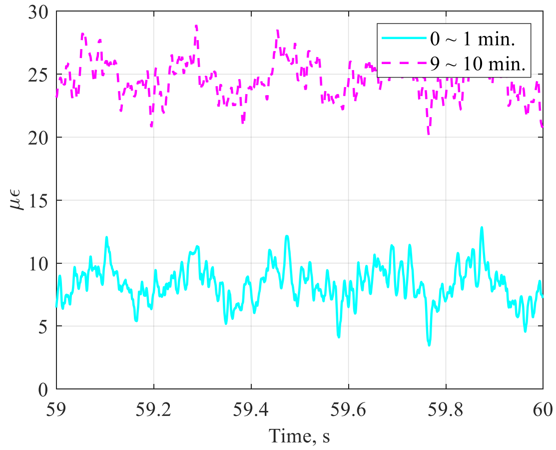

(b) Flap chord-wise gauge

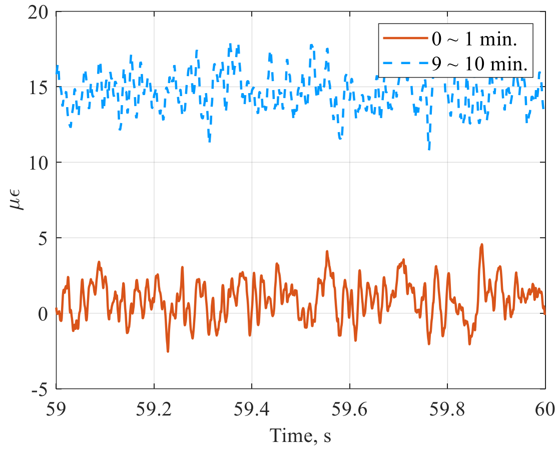

(c) Steel shaft guide gauge

Figure 6. Strains measured in 20kg loading condition

2.3.3. Dynamic characteristics of the flap mechanism under static loads

Piezoelectric actuators generally feature hysteresis nonlinear characteristics. On the other hand, hysteresis depends on the frequency where it imposes a large phase distortion at low frequencies and relatively small phase distortion on high frequencies [16, 17]. The flap response to 1 Hz input signal is plotted in Fig. 7. The plot for two periods are overlapped together, and it is observed that the hysteresis occurs in a regular fashion. There are no amplitude discrepancies between the two periods, and the other periods show the same responses as well.

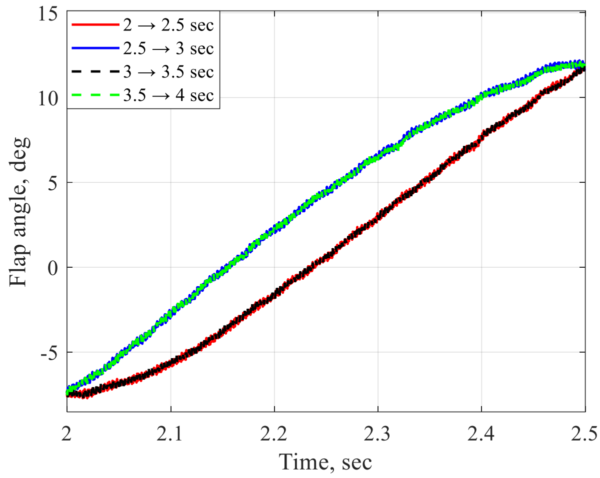

Figure 7. Hysteresis observed at 1 Hz response

Figure 8 shows the frequency response of the present flap mechanism that reveals the nonlinear characteristic of a piezoelectric actuator. Lower frequencies have steady phase delays due to high hysteresis effect, whereas high frequency signal can be regarded as linear. Linear dynamics can be derived for small input voltages at those frequencies, which may be mathematically modeled with the first-order electrical capacitance delay τ and the second-order mechanical properties of m, c, and k. Therefore, parameters of the third-order transfer function are estimated by the least-squares method from the measured step responses or sweeping of the frequency responses.

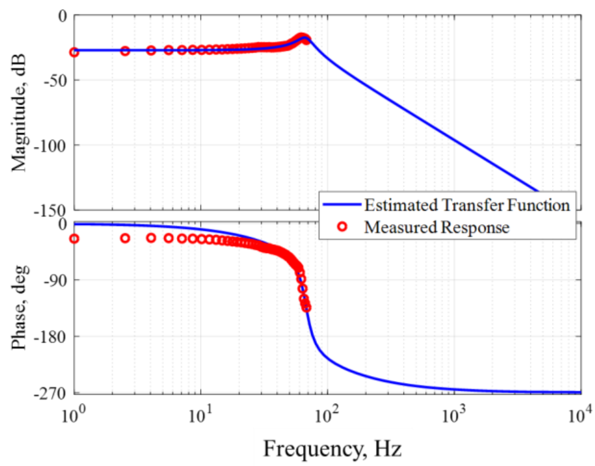

Figure 8. Input voltage to flap angle frequency response

2.3.4. Tensile load test on the blade specimens

Figure 9 shows the load histories and crosshead displacements with time during the tensile test program for both root specimen and flap specimen. The load increases faster in the root specimen case even in the same crosshead speed. This

Presented at 45th European Rotorcraft Forum, Warsaw, Poland, 17-20 September, 2019

This work is licensed under the Creative Commons Attribution International License (CC BY). Copyright © 2019 by author(s).

implies that the axial stiffness of the root specimen is larger than the flap specimen, where indeed the root part has more reinforcement skin plies. In Fig. 9-(a), the load increased linearly up to 20kN, which is the maximum tensile load expected in the trim condition. However, a small matrix crack occurs at 18kN load in the root specimen, as indicated by the small sudden drop of the load at 110 s. Then, a relatively large crack occurs at 24.9kN, and the test is stopped due to the load cell limit on 25kN.
Similar matrix crack is observed for the flap specimen at 15kN. Flap specimen shows more small cracks for load over 20kN, and exhibits a continuous fracture when the load is increased to 24kN. Then, the safety factor of each specimen is derived based on the actual load at which continuous cracking occurs and the expected load from comprehensive rotor analysis using DYMORE as in Eq. (1) [19].

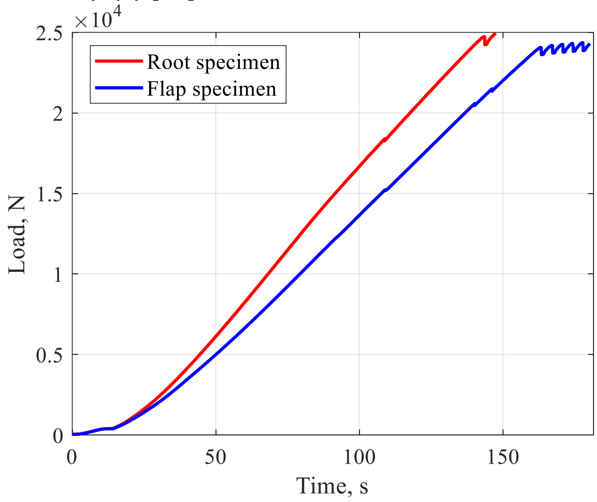

(a) Load histories

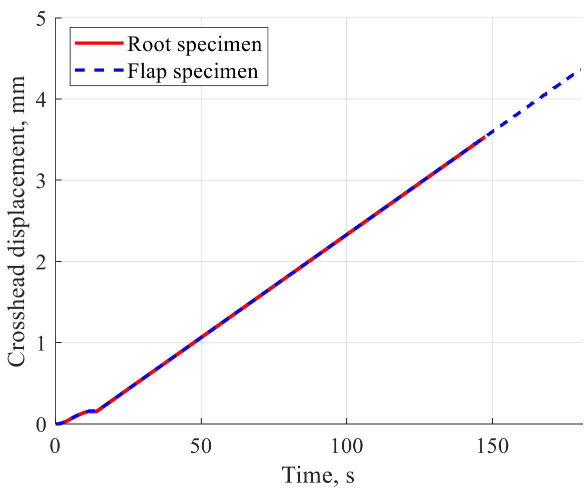

(b) Crosshead displacement histories

Figure 9. Blade tensile loading test results

(1) $$F_S = L_{crack}/L_{analysis}$$

The safety factor estimated by Eq. (1) is 1.42 for root specimen and 1.77 for flap specimen.

Figure 10 shows the strains measured in the tensile load direction. Strain observed for the root specimen is smaller than that observed for the flap specimen at 25% chord. The cracks are detected on exact timing as the load cell measurement. Root specimen shows some strain behaviors similar to plastic deformation before the initial crack at 110 s, revealing the decrease of slope.
Figure 11 shows the measured flap tip deflection with time. The amplitude of the deflection remains the same, but the steady flap tip deflection is affected by the tensile loading and deformation, which implies out-of-plane bending is occurred during the test.

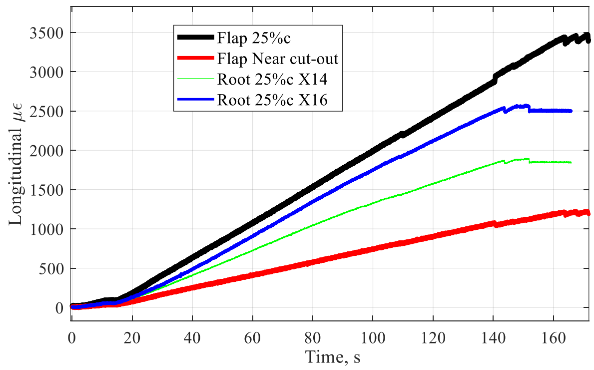

Figure 10. Measured strains

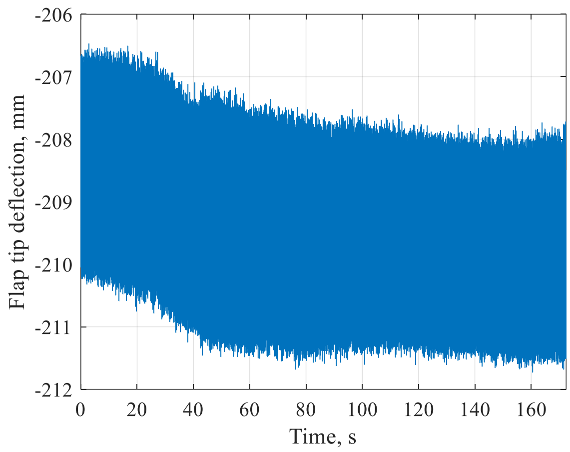

Figure 11. Flap tip displacement history

In summary, the root of the blade may survive at the operating speed of 1,300RPM as the actual centrifugal load is smaller than the tensile loading, with more than 40% safety margin. The integrity of the flap part of the blade is satisfied as the actual centrifugal tensile load will be 15kN. Further, the strain-load relation shows linear elastic behavior under imposed 25kN load range. There are no significant deformation or fractures observed in the outer skin of the specimens after the test.

Presented at 45th European Rotorcraft Forum, Warsaw, Poland, 17-20 September, 2019
This work is licensed under the Creative Commons Attribution International License (CC BY). Copyright © 2019 by author(s).

2.3.5. Correlation with cross-section analysis

Figures 12 and 13 show a load versus strain plot of the root specimen. Estimated equivalent axial stiffness are 1.364×10^7 N for X14 cross-section location, 7.687×10^6 for X18 cross-section, and 9.946×10^6 N for X16 cross-section, respectively. Table 1 summarizes the results of the axial stiffness from measured strain and numerical prediction using VABS. The axial stiffness from the measurement is not the sectional stiffness, for the measured strain is only from the outer skin. Therefore, the stiffness ratios from the measured value and analysis are compared. Stiffness variations in both X14/X16 and X16/X18 have average of 12% difference.

Table 1. Axial stiffness comparison

EA, 10^6 N	VABS analysis	Strain gauge	Percentile difference
X14	15.11	13.64	-
X16	12.49	9.946	-
X18	11.29	7.687	-
X14/X16	1.21	1.37	11.68%
X16/X18	1.11	1.29	13.95%

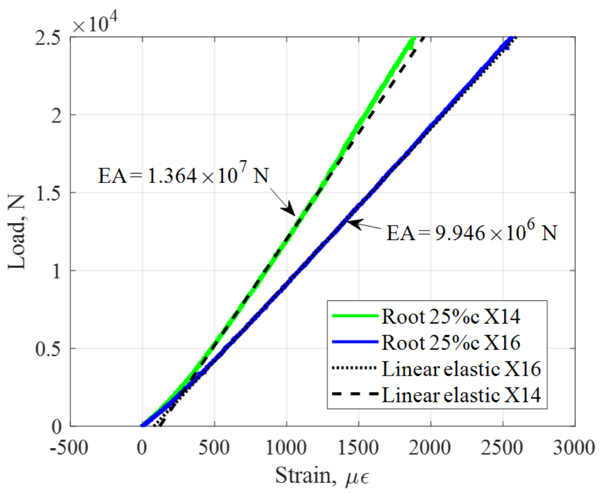

Figure 12. Load-strain and equivalent axial stiffness of the root specimen

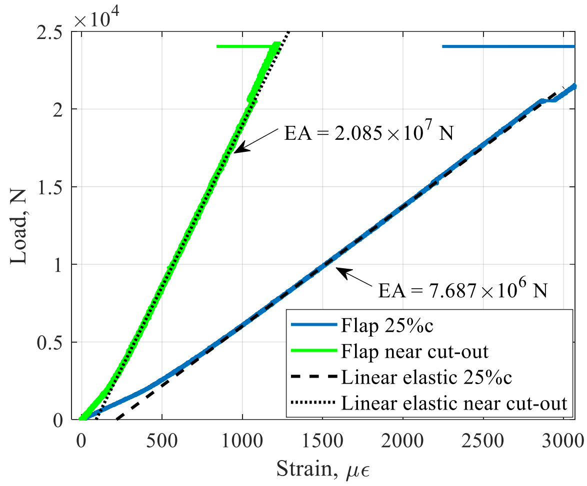

Figure13. Load-strain and equivalent axial stiffness of the flap specimen

2.3.6. Sectional stiffness test

Figure 4-(c) shows the strain gauge installation inside the blade, on both upper and lower innermost layers of the skin. Sectional flap bending stiffness at the root are derived from strains using Eq. (2).

(2) $$EI = (Mh)/(|\varepsilon_1| + |\varepsilon_2|)$$

where ε_1 and ε_2 are strains from upper and lower skin, respectively, and h is the distance of the sensors as plotted in Fig. 4-(c). Sum of each strain $(|\varepsilon_1| + |\varepsilon_2|)$ is directly obtained by multiplying by 2 to the full bridge strain gauges. Also, a root fixing jig and a tip mass create bending moment in the flap-wise direction, which are depicted in Fig. 4-(a). In the case of the torsional stiffness measurement, imposing exact moment to the blade is important. In Fig. 4-(b), a blade clamp and a fixed pulley can impose torsional moment to the blade by the mass hanging on the pulley. However, since the cross-section of the blade has complex shape, the torsional stiffness should be determined considering the out-of-plane warping as in Eq. (3):

(3) $$GJ = Q/\kappa = Q(\frac{\partial\psi}{\partial x_2} - x_3)/(2\varepsilon_{45°})$$

where Q indicates applied moment on the section, κ is the radius of curvature, and x_2 and x_3 are cross-sectional coordinates [20]. Then, only 45° strain is compared with the analytic solution under the same amount of moment as it is not straightforward to determine the warping function $(\partial\psi/\partial x_2 - x_3)$ experimentally.

Figure 14 shows time history of the measured full-bridge bending strains for two different tip loads, and Table 2 summarizes the evaluated flapwise bending stiffness using the steady-state strains and analytical prediction. Average difference between the test and analysis is -3.9%.

Presented at 45th European Rotorcraft Forum, Warsaw, Poland, 17-20 September, 2019

This work is licensed under the Creative Commons Attribution International License (CC BY). Copyright © 2019 by author(s).

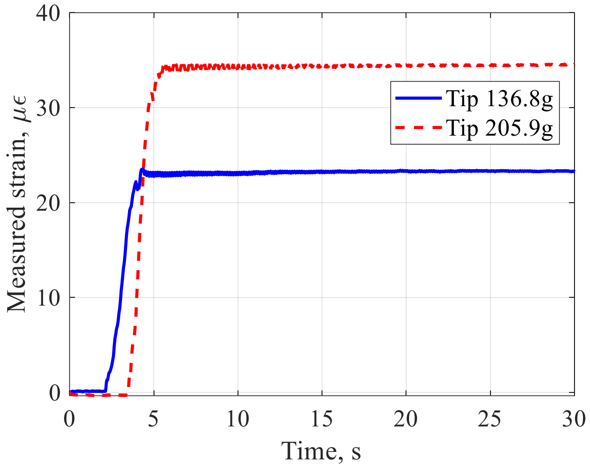

Figure 14. Measured strains for the flap bending stiffness estimation test

Table 2. Flapwise bending stiffness comparison

Case	VABS EI_{flap}, Nm^2	Measured EI_{flap}, Nm^2	Percentile difference
136.8g	339.8	324.42	-4.53
205.9g	339.8	328.63	-3.29

Figure 15 shows time history of the measured half-bridge 45° strain for X14 section under two different moments. Figure 16 shows recovered strain at X14 section from VABS-DYMORE analysis using the same amount of the applied moment. Marked numbers show strains at which strain gauge is installed on the blade. Summary of the results are given in Table 3. Average difference between the test and analysis is 25%.

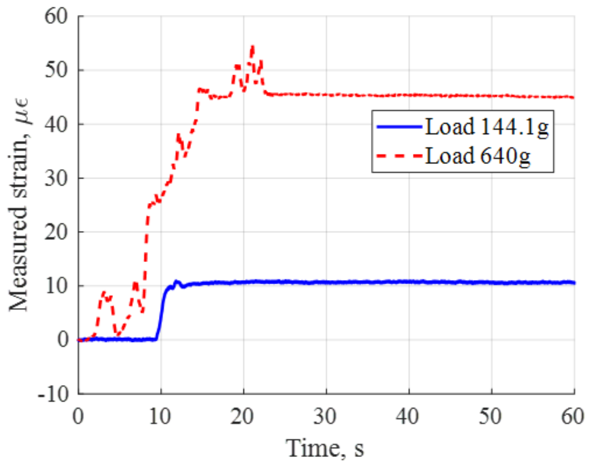

Figure 15. Measured strains for the torsional moment test

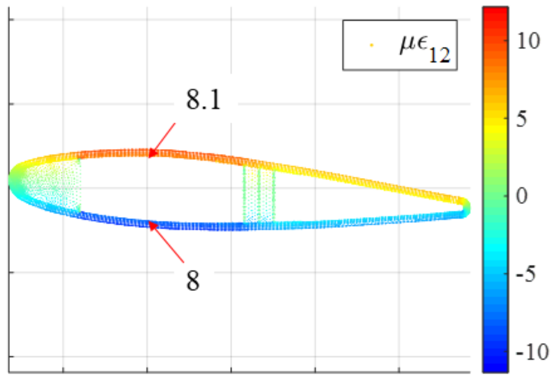

(a) Load 144.1g

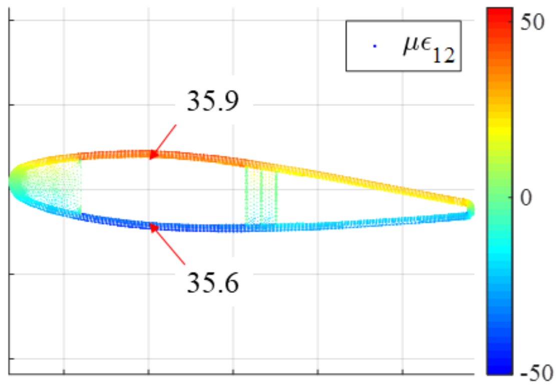

(b) Load 640g

Figure 16. VABS-DYMORE strain recovery for the torsional moment test analysis

Table 3. Torsional moment test

Case	VABS $\mu\varepsilon_{45°}$	Measured $\mu\varepsilon_{45°}$	Percentile difference
144.1g	8	10	25
640g	36	45	25

2.3.7. Modal test

Figure 17 shows the free-free modal frequencies obtained from NASTRAN analysis and the test. It is noteworthy to see that the discrepancy of the first flap bending mode and the first torsion mode in Fig. 17 (b) corresponds to the strain gauge measurements in Tables 2 and 3.

Mode shape vectors are produced by quadrature picking for modal displacement [21]. If the k-th mode shape vector is denoted as $\boldsymbol{\phi_k} = [\phi_{1k}, \ \phi_{2k}, \ \cdots, \ \phi_{nk}]^T$, $\mathrm{k} = 1 \cdots \mathrm{n}$, it will be approximately proportional to $\mathrm{Imag}[H_i(j\omega)]_{\omega=\omega_k}$ where $H_i(j\omega)$ is i-th column of $H(j\omega)$, $\mathrm{i} = 1 \cdots \mathrm{n}$.

Presented at 45th European Rotorcraft Forum, Warsaw, Poland, 17-20 September, 2019
This work is licensed under the Creative Commons Attribution International License (CC BY). Copyright © 2019 by author(s).

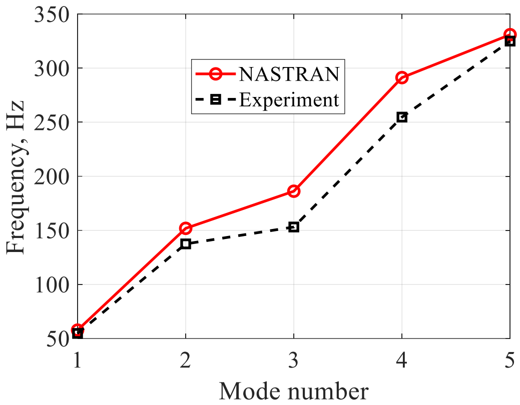

(a) Natural frequencies obtained from NASTRAN and experiment

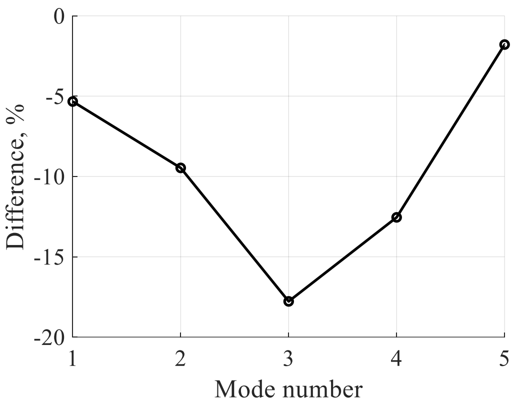

(b) Percentile differences of mode frequencies between NASTRAN and experiment

Figure 17. Natural frequencies comparison

Figure 18 (a)-(d) depict identified mode shapes from experiment, and Fig. 19 (a)-(d) show mode shape calculated from NASTRAN. To evaluate the exact correlations between the modes, the modal assurance criteria (MAC) should be derived using the eigenvectors from test and analysis. The MAC is computed in each eigen frequencies, which is defined as:

$$MAC_{ij} = \left|\psi_i^T \phi_j\right|^2 / [(\phi_j^T \phi_j)(\psi_i^T \psi_i)] \quad (4)$$

where ψ or ϕ are designated as eigenvector from the test or analysis. Figure 20 shows the computed MAC values. MAC value is larger than 0.9 for the first three modes. Since the experiment reveals the coupled flap bending and torsion mode while the analysis has the uncoupled 2nd torsion mode, MAC value for those modes becomes smaller than 0.9. The reason for the discrepancy may be a lack of impact roving points or improper material properties. On the other hand, there are roving nodes of which the frequency bandwidth of the impact force is lower than the fourth mode frequency as shown in Fig. 21. Thus, the present modal test is capable of estimating up to the third mode.

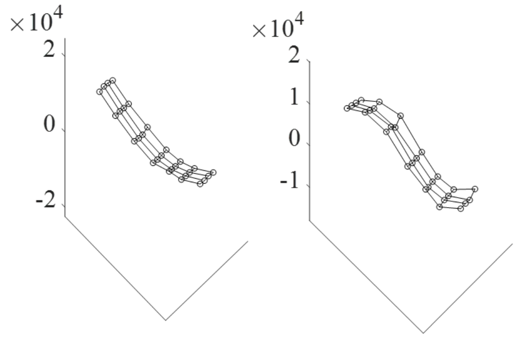

(a) 1st flap bending (b) 2nd flap bending

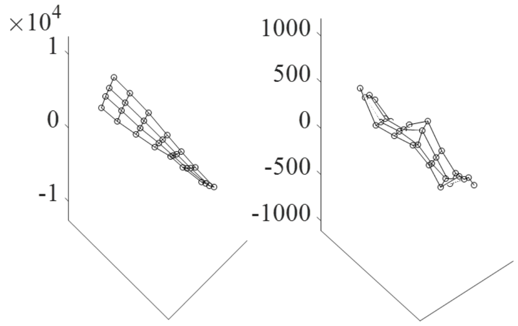

(c) 1st torsion (d) 3rd flap bending

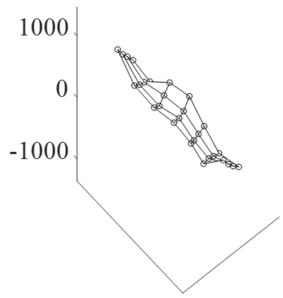

(e) Coupled 3rd flap bending and 2nd torsion

Figure 18. Experimental mode shape

3. CONCLUSION AND FUTURE WORKS

In this paper, recent bench experiment results on the flap mechanism and tensile testing results of the SNUF blade and relevant evaluation are presented. The bench test on the flap mechanism reveals satisfactory strains under the expected centrifugal load, and the dynamic tests shows that the present flap actuation system has 4/rev bandwidth. Tensile testing of the blade shows that it has sufficient safety factor. Also, the axial stiffness ratios had 12% difference between the measurements and VABS cross-sectional analysis. Further, both sectional strain measurements and the identified modal frequencies show similar discrepancies in the flapping and torsional directions, which are 4% and 20% differences with analysis, respectively. Finally, estimated MAC values for the first three fundamental modes satisfy the rejection criteria of 0.9.

In the future, the flap mechanism dynamics and

Presented at 45th European Rotorcraft Forum, Warsaw, Poland, 17-20 September, 2019

This work is licensed under the Creative Commons Attribution International License (CC BY). Copyright © 2019 by author(s).

durability will be tested on Korea Aerospace Research Institute (KARI) hover stand. System identification procedure on the hover stand and wind-tunnel will be implemented. Also, it will be examined if any substantial improvements are required in the blade design or flap mechanism design.

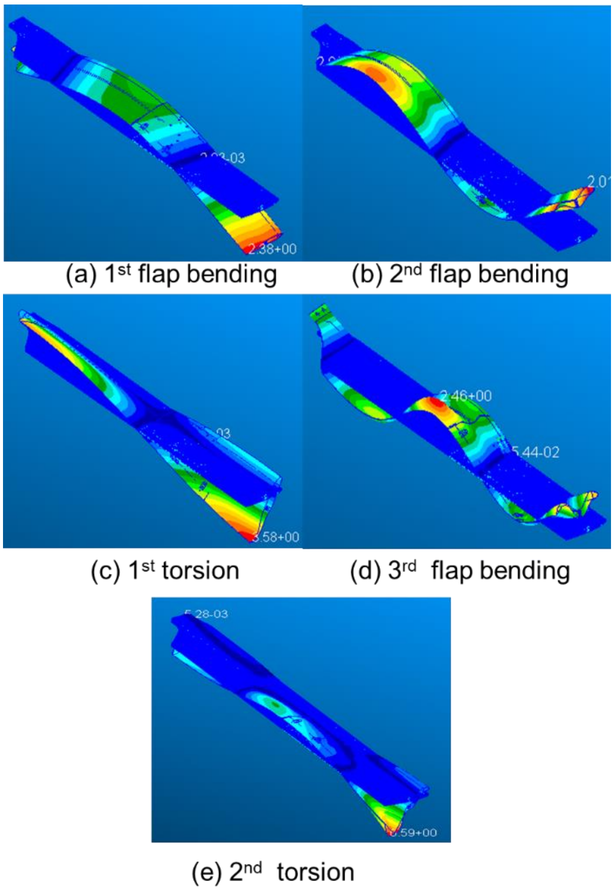

Figure 19. Analytical mode shapes by NASTRAN

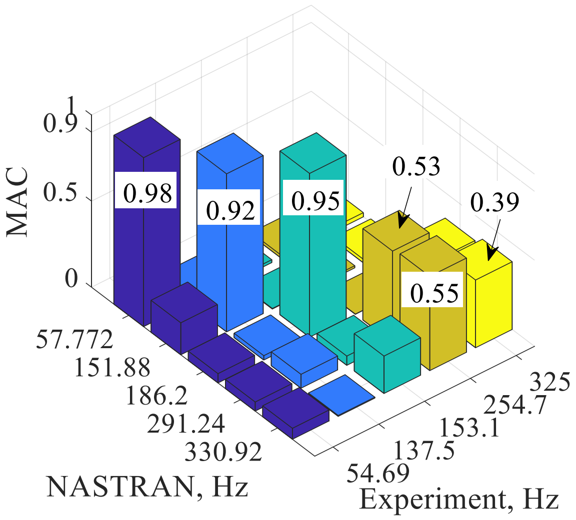

Figure 20. Presently obtained MAC plot

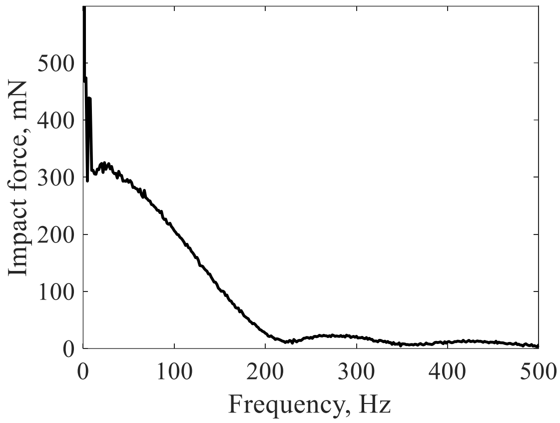

Figure 21. Impact force frequency response for the roving node 11

4. REFERENCES

[1] Ham, N. D., "Helicopter Individual Blade Control and Its Applications," American Helicopter Society 38th Annual Forum Proceedings, St. Louis, MO, 1983.

[2] Shin, S. J., Cesnik, C. E. S., and Hall, S. R., "Closed-Loop Control Test of NASA/ARMY/MIT Active Twist Rotor for Vibration Reduction," Journal of the American Helicopter Society, Vol. 50, (2), 2005, pp. 178–194. doi: 10.4050/1.3092854

[3] Friedmann, P. P., "On-Blade Control of Rotor Vibration, Noise, and Performance: Just Around the Corder? The 33rd Alexander Nikolsky Honorary Lecture," American Helicopter Society 69th Annual Forum, Phoenix, AZ, May 2013. doi: 10.4050/JAHS.59.041001

[4] Koratkar, N. A., and Chopra, I., "Open-Loop Hover Testing of a Smart Rotor Model," AIAA Journal, Vol. 40, (2), August 2002, pp. 1495–1502. doi: 10.2514/2.1834

[5] Koratkar,N.A., and Chopra, I., "Wind Tunnel Testing of a Smart Rotor Model with Trailing Edge Flaps," Journal of the American Helicopter Society, Vol. 47, (4), October 2002, pp. 263–272. doi: 10.4050/JAHS.47.263

[6] Roget, B., and Chopra, I., "Closed-Loop Test of a Rotor with Individually Controlled Trailing-Edge Flaps for Vibration Reduction," Journal of the American Helicopter Society, Vol. 55, (1), 2010, pp. 1-10. doi: 10.4050/JAHS.55.012009

[7] Straub, F. K., Anand, V. R., Birchette, T. S., and Lau, B. H., "SMART Rotor Development

This work is licensed under the Creative Commons Attribution International License (CC BY). Copyright © 2019 by author(s).

and Wind Tunnel Test," 35th European Rotorcraft Forum, Hamburg, Germany, Sept. 2009.

[8] Roth, D., Enekl, B., and Dieterich, O., "Active Rotor Control by Flaps for Vibration Reduction - Full Scale Demonstrator and First Flight Test Results," Proceedings of 32nd European Rotorcraft Forum, Maastricht, The Netherlands, September 12–14, 2006.

[9] Padthe, A. K., Friedmann, P. P., and Prasad, J. V. R., "High-Fidelity Linear Time-Invariant Models for Higher Harmonic Closed-Loop Rotor Control Studies," Journal of the American Helicopter Society, Vol. 62, (012003), 2017, pp. 1-15, doi: 10.4050/JAHS.62.012003

[10] Eun, W. J., Sim, J. S., Lee, S. W., and Shin, S. J., "Advancement of the SNUF Blade Design through Flap Configuration Parametric Study and Optimization Framework," AHS International 73rd Annual Forum & Technology Display, Fort Worth, Texas, May 9-11, 2017.

[11] Eun, W. J., Im, B. U., and Shin, S. J., "Endurance Test of the Revised SNUF blade with Active Trailing-Edge Flap," The 6th Asian/Australian Rotorcraft Forum / Heli Japan, Kanazawa, Japan, November, 2017.

[12] Visconti, U., Eun, W. J., Sim, J. S., Lee, S. W., and Shin, S. J., "Design Improvements and Flap Deflection Evaluations with Considering Centrifugal Load on Active Trailing Edge Flap," Aircraft Engineering and Aerospace Technology, 2017.

[13] Eun, W. J., Sim, J. S., Lee, S. W. and Shin, S. J., "Further Improvements in the SNUF Blade Design by Numerical Design Optimization Framework," ASCE's Journal of Aerospace Engineering, 2018.

[14] Im, B. U., Lee, C. B., Eun, W. J., and Shin, S. J., "System Identification of SNUF Blade Equipped with an Active Trailing-Edge Flap," The 7th Asian/Australian Rotorcraft Forum, Jeju Island, Korea, October, 2018.

[15] Kumar, D., Design and Analysis of Composite Rotor Blades for Active/Passive Vibration Reduction, Ph.D. Thesis, University of Michigan, 2013.

[16] Lee, T., and Chopra, I., "Design of piezostack-driven trailing-edge flap actuator for helicopter rotors," Smart Materials and Structures, Vol. 10, (1), May. 2000, pp. 15–24.

[17] Zhu, W., and Rui, X. T., "Hysteresis modeling and displacement control of piezoelectric actuators with the frequency-dependent behavior using a generalized Bouc-Wen model," Precision Engineering, Vol. 43, (31), Jan. 2016, pp. 299–307.

[18] Yu, W., and D. H. Hodges, "Generalized Timoshenko Theory of the Variational Asymptotic Beam Sectional Analysis," Journal of the American Helicopter Society, Vol. 50, (1), 2005, pp. 46–55. doi: 10.4050/1.3092842

[19] Bauchau, O. A., "Flexible Multibody Dynamics," Springer, Dordrecht, Heidelberg, London, NewYork, 2011.

[20] Bauchau O. A. and Craig J. I., "Structural Analysis with applications to aerospace structures," Springer Netherlands, 2009.

[21] Lecture Note of NOVIC(Noise and Vibration Control) Seminar: Modal Analysis: Theory, Testing and Applications, KAIST, Daejeon, June 2019.

This work is licensed under the Creative Commons Attribution International License (CC BY). Copyright © 2019 by author(s).